A Broadband UHF Near-Field RFID Antenna

Xianming Qing, *Member, IEEE*, Chean Khan Goh, and Zhi Ning Chen, *Fellow, IEEE*

***Abstract*—A broadband segmented loop antenna is presented for ultra high frequency (UHF) near-field radio frequency identification (RFID) applications. Using a segmented line, the current distribution along the loop is kept in phase even though the perimeter of the loop is more than two operating wavelengths so that the proposed antenna generates strong and even magnetic field distribution in the near-field zone of the antenna. The antenna prototype, printed onto a piece of FR4 substrate, with an overall size of $175 \times 180 \times 0.5\ \mathrm{mm}^3$, achieves a large interrogation zone of $154 \times 154\ \mathrm{mm}^2$ with good impedance matching and uniform magnetic field distribution over the entire UHF RFID band of 840–960 MHz.**

***Index Terms*—Antenna, loop antenna, near-field antenna, radio frequency identification (RFID), segmented loop antenna, UHF.**

I. Introduction

RADIO frequency identification (RFID), which was developed around World War II, is a technology that provides wireless identification and tracking capability [1], [2]. RFID systems employ semiconductor-based wireless technology to identify and track objects. Such systems enable us to simultaneously read/write multiple tags and activate remote sensing devices based on their unique IDs conveniently and selectively [3]. Currently, ultra-high frequency (UHF) near-field RFID technology receives a lot of attention due to the promising opportunities in item-level RFID applications such as sensitive products tracking, pharmaceutical logistics, transport and medical products (blood, medicines, vaccines), bio-sensing applications (biohazard materials, security, etc.), and so on [4]–[8].

One of the challenges in UHF near-field RFID applications is to design reader antennas with a large interrogation zone. The conventional solid-line loops have been used as reader antennas in low frequency (LF)/high frequency (HF) RFID systems for many years. Usually, these electrically small loops (i.e. the perimeter of a loop antenna $\mathrm{C} < \lambda/2\pi$, where λ is the operating wavelength) can produce strong and uniform magnetic field in the region near to the antenna. However, UHF RFID applications require a reader antenna with a large coverage (for example, $150 \times 150\ \mathrm{mm}^2$). The loop antenna which offers such a large interrogation zone is no longer electrically small. The conventional solid-line loop with the perimeter comparable to one operating wavelength cannot produce even magnetic field distribution in the near-field zone of the antenna because the current distribution along the loop experiences phase-inversion and current nulls. The magnetic field is relatively weak in certain region of the interrogation zone, which degrades the reliability of RFID tag detection.

Some electrically large loop antennas have been reported to generate strong and even magnetic filed. Dobkin *et al.* presented a segmented magnetic antenna consisting of a number of segments and each segment is composed of a metal line and a series lumped capacitor in 2007 [12]. A segmented loop antenna with a diameter of 10 cm demonstrated desirable performance at 915 MHz. Oliver proposed the broken-loop antennas in 2008. Three broken-loop antennas using different coupled lines, namely triple line, double line and single line, were conceptually demonstrated in the U.S. design patents [13]–[15].

In this paper, a segmented loop antenna is presented to generate strong and even magnetic field distribution in a large near-field zone for broadband UHF near-field RFID applications. The proposed antenna is investigated numerically and validated experimentally. The methodology to implement the antenna with impedance matching network is addressed with the practical guideline. The extensive parametric studies are carried out to explore the operating mechanism of the antenna and provide useful information for antenna optimization.

This paper is organized as follows. Section II gives a brief review of the UHF near-field RFID systems. Section III presents the configuration of the proposed segmented loop antenna. In Section IV, the parametric studies are carried out to investigate the effect of geometrical parameters on the antenna performance. The antenna prototype and the results are exhibited in Section V. Finally, Section VI provides a summary.

II. UHF Near-Field RFID

The basic concern of UHF near-field RFID is to make the RFID system working in a short distance as reliable as that of the LF/HF near-field RFID [4]. Similar to the LF/HF RFID systems, a UHF near-field RFID reader antenna and tags can be coupled either magnetically (inductively) or electrically (capacitively) [9]. Inductive coupling systems are preferred in most of the applications since most of the reactive energy is stored in the magnetic field. Such systems are only affected by the objects with high magnetic permeability and are able to operate in close proximity to metal and liquid. In contrast, capacitive coupling systems are hardly used in the practical applications because the energy is stored in the electric field which is severely affected by the objects with high dielectric permittivity.

In an inductive coupling RFID system, the reader and the tag antennas are coupled mainly through the magnetic field. If the tag antenna is electrically small, the magnetic field generated by the reader antenna is hardly perturbed by the tag, and

Manuscript received January 07, 2010; revised May 11, 2010; accepted June 11, 2010. Date of publication September 23, 2010; date of current version November 30, 2010. The work was supported by Agency for Science, Technology and Research (A*STAR), Singapore.

The authors are with the Institute for Infocomm Research, Singapore, Agency of Science, Technology, and Research, Singapore 138642, Singapore (e-mail: qingxm@i2r.a-star.edu.sg; ckqoh@i2r.a-star.edu.sg; chenzn@i2r.a-star.edu.sg).

Color versions of one or more of the figures in this paper are available online at http://ieeexplore.ieee.org.

Digital Object Identifier 10.1109/TAP.2010.2078432

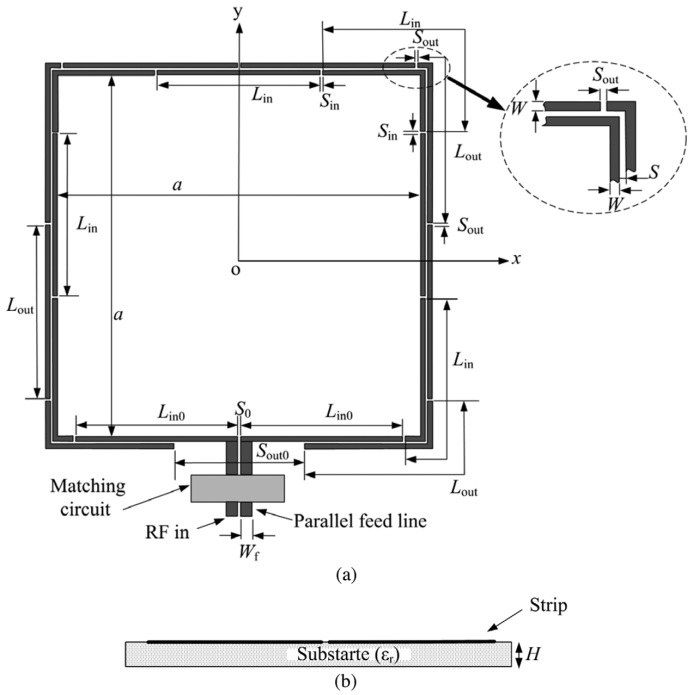

Fig. 1. Configuration of the proposed segmented loop antenna: (a) top view and (b) side view.

the coupling coefficient, C, is affected by the following factors [10], [11]

$$C \propto f^2 N_{tag}^2 S_{tag}^2 B^2 \alpha \tag{1}$$

where f is operating frequency, $N_{\rm tag}$ is the number of the turns of the coil tag antenna, $S_{\rm tag}$ is the cross-section area of the coil, B is the magnetic field density at the tag location generated by the reader antenna, and α is the antenna misalignment loss. Formula (1) indicates that the coupling in a near-field RFID system with a coil tag is dependent on the magnetic field density generated by the RFID reader antenna. A reader antenna that can produce strong and even magnetic field in an interrogation zone will enhance the reading rate as well as the reliability of the system and is thus desired in UHF near-field RFID systems.

III. Antenna Configuration

The proposed segmented loop antenna is shown in Fig. 1. A Cartesian coordinate system is oriented such that the upper surface of a substrate lies in $x-y$ plane and the center of the square segmented loop is at the origin of the coordinate system. The antenna is fed by a parallel strip line with a strip width of $W_{\rm f}$ and a separation of S_0. A matching circuit is used to achieve the antenna impedance matching over a required frequency range.

The antenna comprises two square dash-line loops which are symmetrically structured with respect to the y-axis. The inner dash-line loop is composed of several line sections with the identical length except the first two sections which are connected to the parallel feed line. The internal area $(a \times a)$ of the inner dash-line loop is indicated as the interrogation zone with a perimeter of $4a$. As shown in Fig. 1, the inner loop has the parameters: the line width, W; the spacing between adjacent line sections, $S_{\rm in}$; and the lengths of dash-line sections, $L_{\rm in0}$ and $L_{\rm in}$. The outer dash-line loop is open-ended and with the parameters of W, $S_{\rm out}$, $S_{\rm out0}$ and $L_{\rm out}$, respectively. The lengths of all the dash-line sections of the outer loop are the same. These two dash-line loops with a separation of S are positioned in such a way that the broken points of the inner loops are located around the middle points of the dash-line sections of the outer loop separately, and vice versa. The segmented coupled line sections are able to provide a very small phase delay between the adjacent sections so that the current flowing along the segmented lines is kept in a single direction. In other words, the current distribution on the segmented loop looks in-phase. Therefore, the segmented loop antenna produces uniform magnetic field distribution even though the loop is electrically large.

For a specific antenna design with the required interrogation zone $(a \times a)$, and the required operating frequency (f_0), the geometrical parameters of the proposed segmented loop antenna can be determined by the following procedures.

1) Length of the excited line sections of the inner dash-line loop $(L_{\rm in0})$: considered as a loaded dipole antenna with an arm length of $L_{\rm in0}$, usually, the length is around 0.2λ, where λ is the operating wavelength.
2) Length of the line sections of the inner dash-line loop $(L_{\rm in})$: based on the perimeter of the interrogation zone $(4a)$, the number of the line sections (N), the width of the line sections (W), and the spacing between the adjacent line sections $(S_{\rm in})$, the length of the inner dash-line sections can be calculated by

$$L_{in} = \frac{4a + 8W - 2L_{in0} - S_0 - (\mathrm{N}+1)S_{in}}{\mathrm{N}}. \tag{2}$$

3) Length of the line sections of the outer dash-line loop $(L_{\rm out})$: the outer dash-line loop is composed of $N+1$ line sections with length of $L_{\rm out}$. Similarly, the length of the dash-line sections can be calculated by

$$L_{out} = \frac{4a + 16W + 8S - S_{out0} - \mathrm{N}S_{out}}{\mathrm{N}+1} \tag{3}$$

where the open-ended spacing, $S_{\rm out0}$, is suggested to be 0.2λ in the design.

It is suggested that the lengths of the dash-line sections, $L_{\rm in}$ and $L_{\rm out}$, are $\sim 0.25\lambda$. In addition, the separation parameters, namely, $S_{\rm in}$, $S_{\rm out}$, S_0, and S, should be electrically small to ensure strong coupling between the segmented coupled lines.

IV. Parametric Studies and Analysis

The parametric studies are carried out to provide readers with more design information. After extensive simulations, it is found that the length of the segmented line section, i.e. the lengths of inner and outer dash-line section, $L_{\rm in}$ and $L_{\rm out}$, and the substrate parameters $(\varepsilon_{\rm r}, H)$ affect antenna performance significantly whereas the other parameters show slight effects. To better understand the influence of these parameters on the antenna performance in terms of the operating frequency and magnetic field distribution, only one parameter is varied at a time while the others are kept unchanged unless indicated. The parametric studies were carried out by simulation. All the simulations were performed using IE3D software which is based on the method of moments [16].

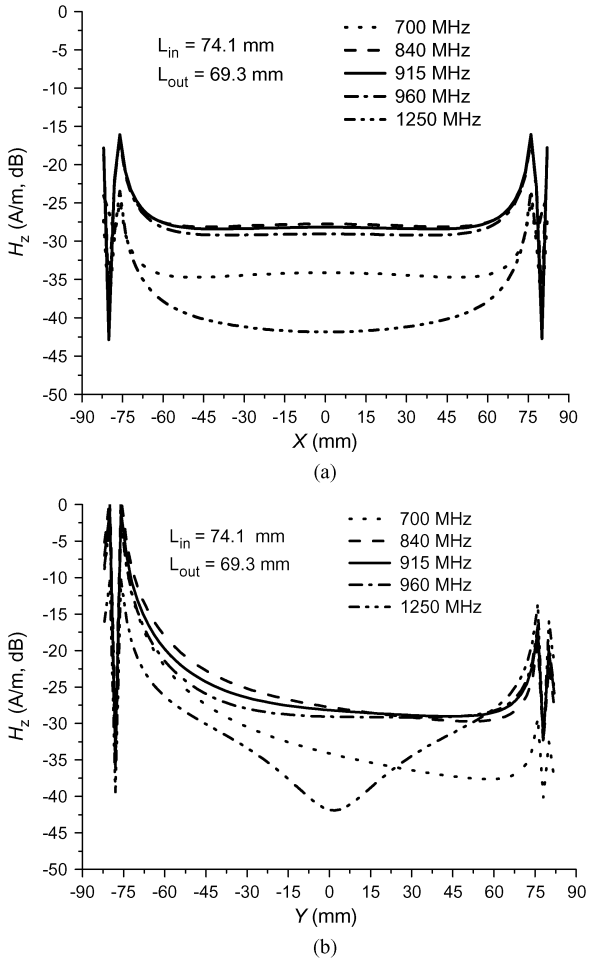

Fig. 2. Simulated magnetic field distribution of the segmented loop antenna at different frequencies with $L_{\rm in} = 74.1$ mm, $L_{\rm out} = 69.3$ mm, $z = 0.5$ mm: (a) x-axis variation and (b) y-axis variation.

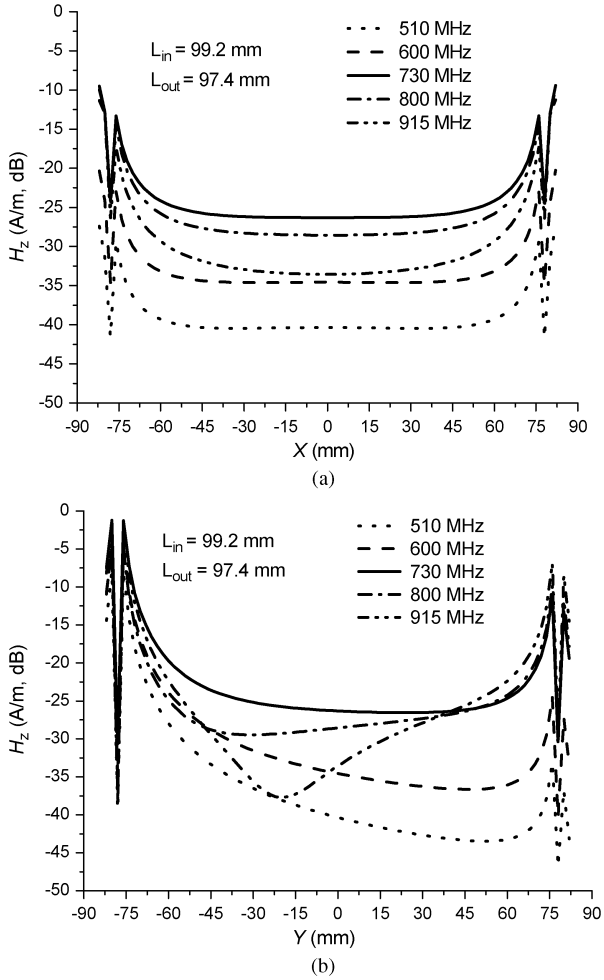

Fig. 3. Simulated magnetic field distribution of the segmented loop antenna at different frequencies with $L_{\rm in} = 99.2$ mm, $L_{\rm out} = 97.4$ mm, $z = 0.5$ mm: (a) x-axis variation and (b) y-axis variation.

A segmented loop antenna with the geometrical parameters: $a = 154$ mm, $N = 7$, $W = 2$ mm, $S = 1$ mm, $L_{\rm in0} = 68.8$ mm, $S_0 = 1.3$ mm, $L_{\rm in} = 74.1$ mm, $S_{\rm in} = 1$ mm, $L_{out} = 69.3$ mm, $S_{\rm out0} = 59.9$ mm, and $S_{\rm out} = 1$ mm, is selected as a reference. The antenna is first designed in free space ($\varepsilon_{\rm r} = 1$, $H = 0$ mm). No feeding line and matching circuit are considered to avoid the possible influence on current distribution of the segmented loop antenna. The feed is placed directly across the feeding sections of the inner dash-line loop.

A. Lengths of the Segmented Line Sections, L_{in} and L_{out}

Figs. 2 to 4 show the magnetic field distributions of the segmented loop antennas with different $L_{\rm in}$ and $L_{\rm out}$, respectively. It is observed that the operating frequency at which the proposed antenna can generate the strongest and the most even magnetic field distribution is strongly dependent on the electrical length of the segmented line section. Table I lists the centre operating frequency, f_0, and the corresponding lengths, $L_{\rm in}$ and $L_{\rm out}$, for all the antennas. It is found that $L_{\rm in}$ and $L_{\rm out}$ are around one quarter wavelength at f_0 in free space.

In addition, sharp field reduction is observed over the intervals of (-80 mm $\leq x \leq -79$ mm or 79 mm $\leq x \leq 80$ mm) and (-80 mm $\leq y \leq -79$ mm or 79 mm $\leq y \leq 80$ mm) where the positions are in between the inner and outer dash-line loops. The sharp reduction happens as the same directed currents on the coupled lines produce opposite directed magnetic fields which cancel each other in the gap between the inner and outer coupled lines.

B. Effect of the Size of the Antenna

Fig. 5 exhibits the magnetic field distribution of the antennas with varying size. The antennas are configured with identical segmented line configuration. The perimeter of the antenna interrogation zone is changed from 0.81λ to 2.95λ (λ is the free space wavelength at 915 MHz). It is observed that all the antennas generate flat magnetic field distribution along the x-axis in the major portion of the interrogation zone. Besides that, the magnetic field intensity of the antenna decreases as the size increases. The magnetic field shows larger variation along the y-axis, the bigger the antenna, the larger the variation. Fig. 6 shows the magnetic field distribution along the z-axis. The smaller antenna generates stronger magnetic field in the region near the antenna and features faster field reduction as the distance increases. In practical applications, there is a trade-off between the interrogation zone and the magnetic field intensity. Smaller antenna generates stronger magnetic field intensity

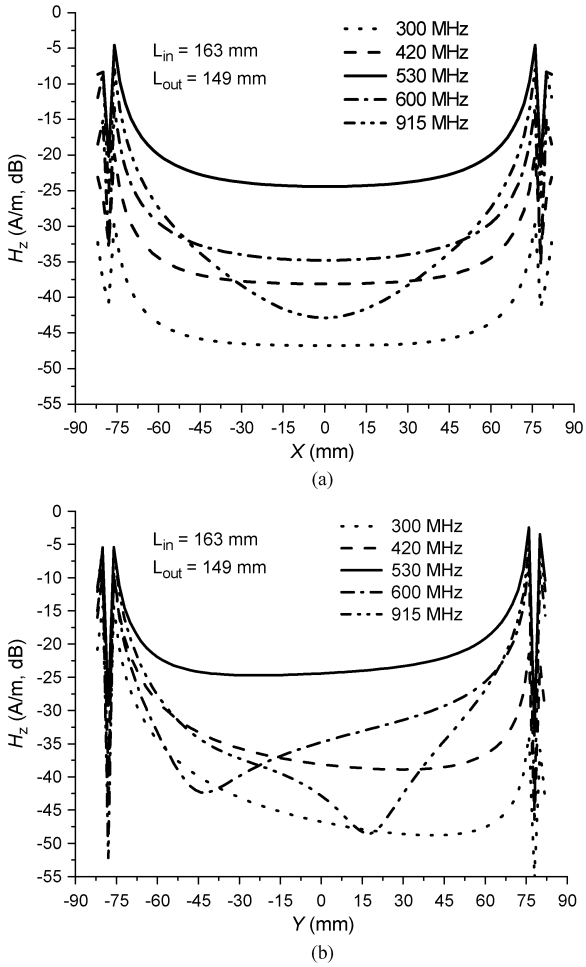

Fig. 4. Simulated magnetic field distribution of the segmented loop antenna at different frequencies with $L_{\rm in} = 163$ mm, $L_{\rm out} = 149$ mm, $z = 0.5$ mm: (a) x-axis variation and (b) y-axis variation.

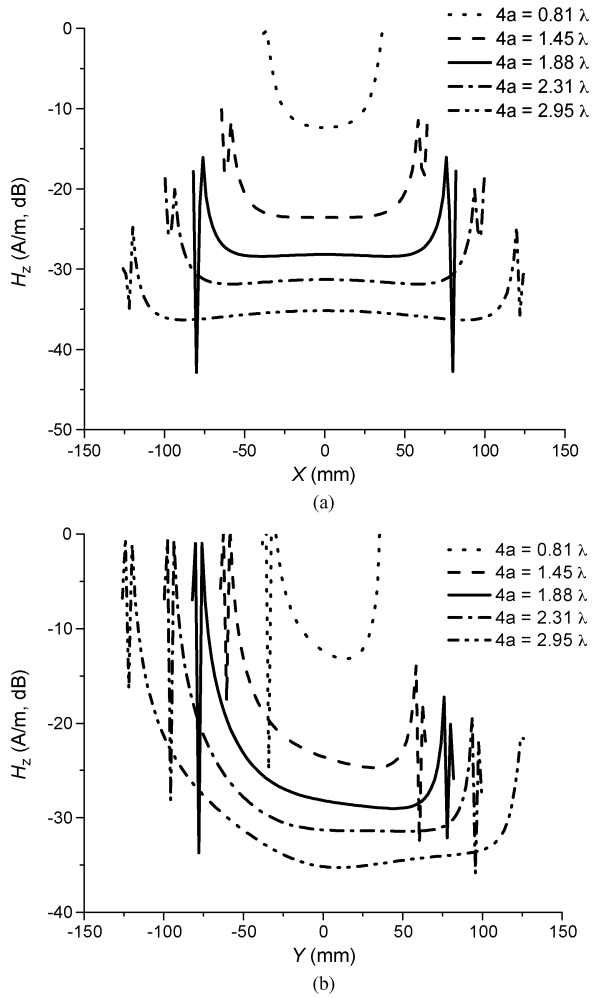

Fig. 5. Simulated magnetic field distribution of the segmented loop antennas with different size at 915 MHz and $z = 0.5$ mm: (a) x-axis variation and (b) y-axis variation.

TABLE I
RELATIONSHIP BETWEEN THE OPERATING FREQUENCY AND THE LENGTHS OF THE SEGMENTED LINE SECTIONS

$L_{\rm in}$ (mm)	$L_{\rm out}$ (mm)	f_0 (MHz)	$\theta_{\rm in}$ (λ)	$\theta_{\rm out}$ (λ)
74.1	69.3	915	0.226	0.211
99.2	97.4	730	0.241	0.237
163	149	530	0.26	0.28

over a limited interrogation zone. The larger antenna achieves a bigger interrogation zone but produces weaker magnetic field intensity.

C. Dielectric Constant $(\varepsilon_{\rm r})$ and Thickness (H) of the Substrate

In practical design, it is convenient and cost effective to print the antenna onto a substrate with a specific dielectric constant $(\varepsilon_{\rm r})$ and a thickness (H). The occurrence of the substrate affects the coupling between the segmented line sections and thus changes the operating frequency of the antenna. The effects of four typical substrates, namely, RT5880 ($\varepsilon_{\rm r} = 2.2$, $\tan\delta = 0.0009$), RO4003 ($\varepsilon_{\rm r} = 3.38$, $\tan\delta = 0.0027$), FR4 ($\varepsilon_{\rm r} = 4.4$, $\tan\delta = 0.02$), and RO3010 ($\varepsilon_{\rm r} = 10.2$, $\tan\delta = 0.0023$), on the antenna operating frequency and magnetic field distribution are investigated for $H = 0.508$ mm.

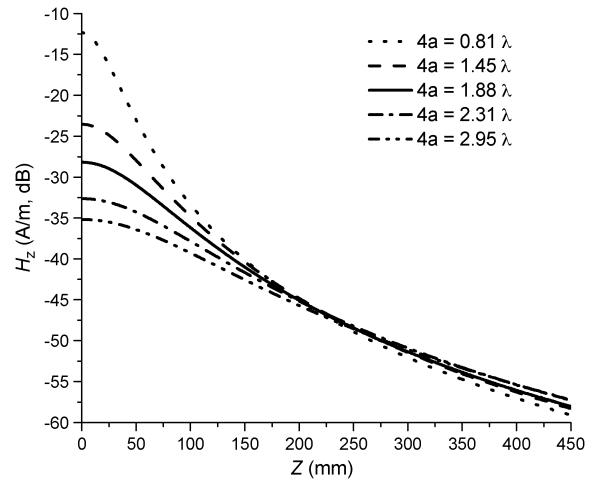

Fig. 6. Simulated magnetic field distribution of the segmented loop antennas along z-axis at 915 MHz.

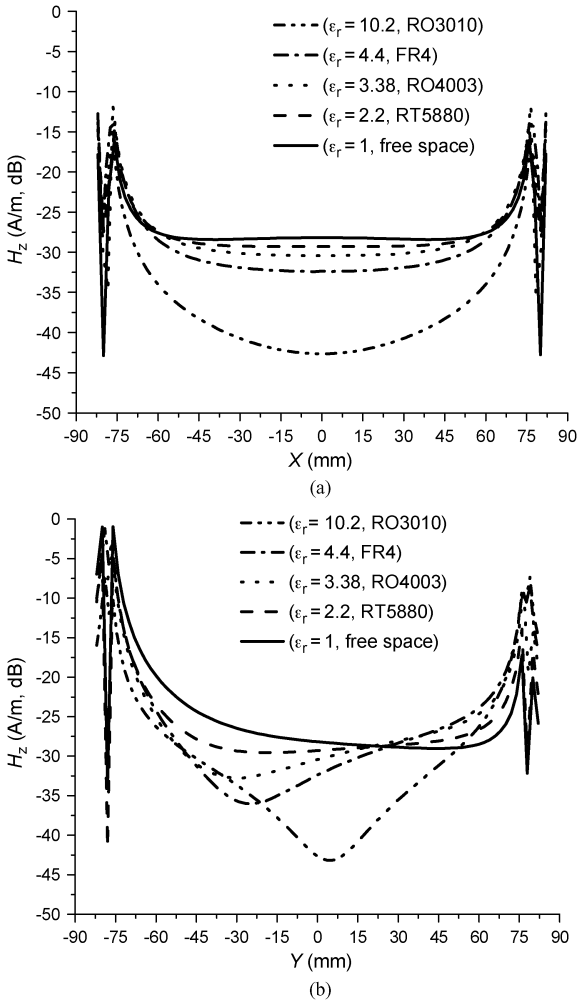

Fig. 7. Effect of the substrate dielectric constant on magnetic field distribution of the segmented loop antenna at 915 MHz and $z = 0.5$ mm: (a) x-axis variation and (b) y-axis variation.

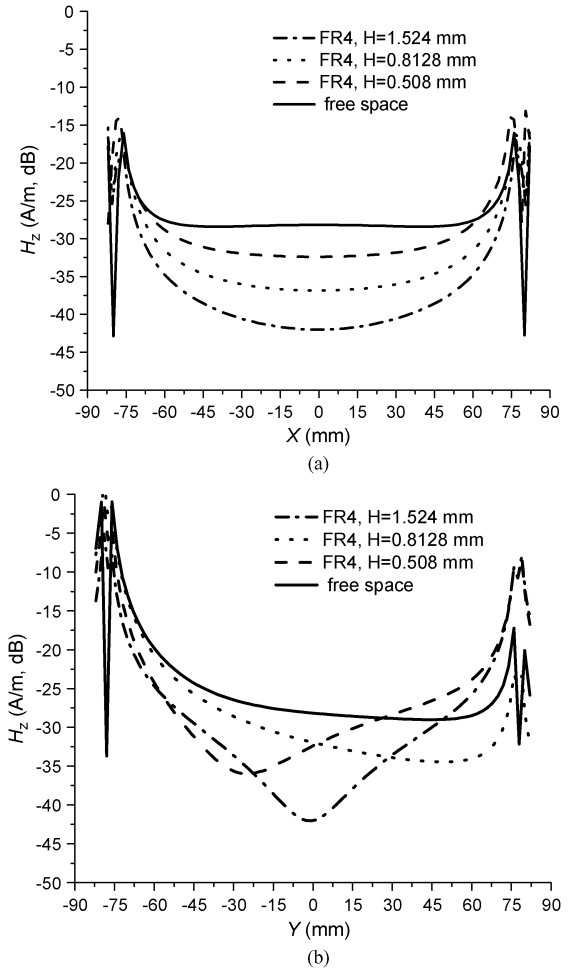

Fig. 8. Effect of the substrate thickness on magnetic field distribution of the segmented loop antenna at 915 MHz and $z = 0.5$ mm: (a) x-axis variation and (b) y-axis variation.

Fig. 7 illustrates the magnetic field distribution for the proposed antenna printed onto different substrates. It is seen that the substrate has significant effect on the magnetic field distribution, which tends to be uneven with the introduction of the substrate. Larger dielectric constant results in larger field variation. The reason is that the introduction of the substrate shifts the operating frequency of the antenna. Further study shows that the operating frequency is shifted to 780 MHz ($\varepsilon_{\rm r} = 2.2$), 740 MHz ($\varepsilon_{\rm r} = 3.38$), 700 MHz ($\varepsilon_{\rm r} = 4.4$), and 580 MHz ($\varepsilon_{\rm r} = 10.2$) for the four substrates, respectively. It implies that the substrate with higher dielectric constant makes the segmented coupled line sections to be electrically longer so that the operating frequency of the antenna is shifted down.

The thickness of the substrate shows a significant effect on the operating frequency as well. Fig. 8 compares the magnetic field distribution of the antennas on FR4 substrate with different thickness at 915 MHz. Similar to the case of increasing the dielectric constant, thicker dielectric substrate raises the effective dielectric constant, and causes the operating frequency to be shifted down. In the examples, the operating frequencies are moved to 610, 660, and 700 MHz for the thickness of 1.524 mm (60 mils), 0.8128 mm (32 mils), and 0.508 mm (20 mils), respectively.

D. Other Parameters

Beside the parameters discussed previously, the effects of the other parameters of the proposed antenna, including the width of the coupled line (W), the spacing between the inner and outer coupled strips (S), the gap between the adjacent lines of the inner and outer dash-line loop ($S_{\rm in}$ and $S_{\rm out}$) were investigated as well for a set of parameters of $W = 0.5$, 1.0, 2.0, 4.0 mm, $S = 0.5$, 1.0, 2.0, 4.0 mm, and $S_{\rm in} = S_{\rm out} = 0.1$, 0.5, 1.0, 1.5, 2.0 mm. These parameters hardly affect the current distribution and the magnetic field distribution of the antenna but to some degree affect the antenna input impedance. In general, these parameters should be electrically small to ensure strong coupling between the coupled lines.

V. Antenna Implementation, Results and Discussion

The proposed segmented loop antenna can be printed onto any substrate and optimized at specific operating frequency by selecting the geometrical parameters properly. In this paper, an antenna prototype which is printed onto a piece of FR4 substrate ($\varepsilon_{\rm r} = 4.4$, $\tan\delta = 0.02$, thickness $H = 0.5$ mm) is demonstrated. The optimized antenna is designed at a center operating frequency of 915 MHz. The antenna prototype is with an overall

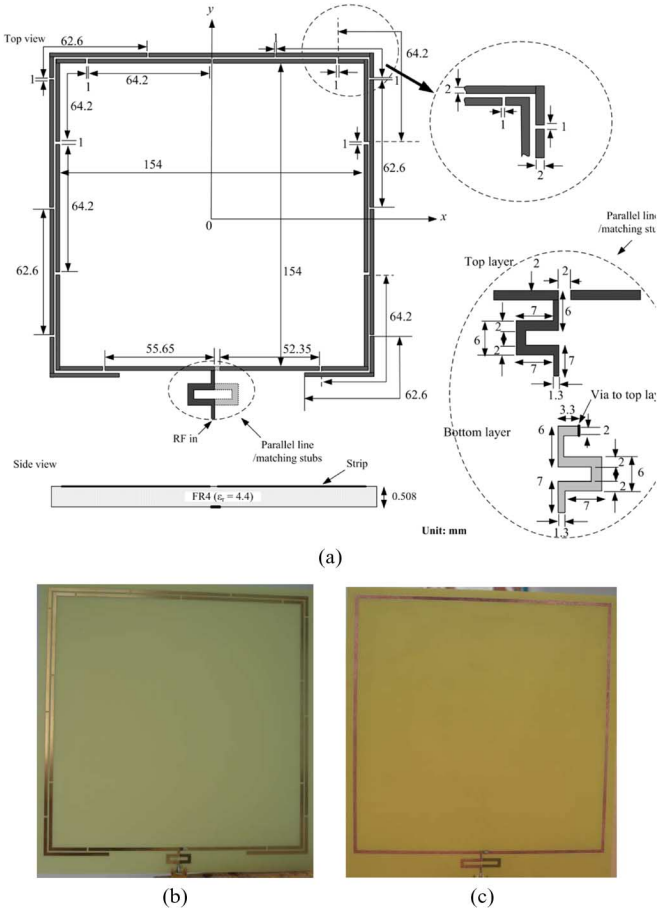

Fig. 9. Loop antennas: (a) detailed dimensions of the segmented loop antenna using FR4 substrate, (b) photo of the segmented loop antenna prototype, and (c) photo of the solid-line loop antenna.

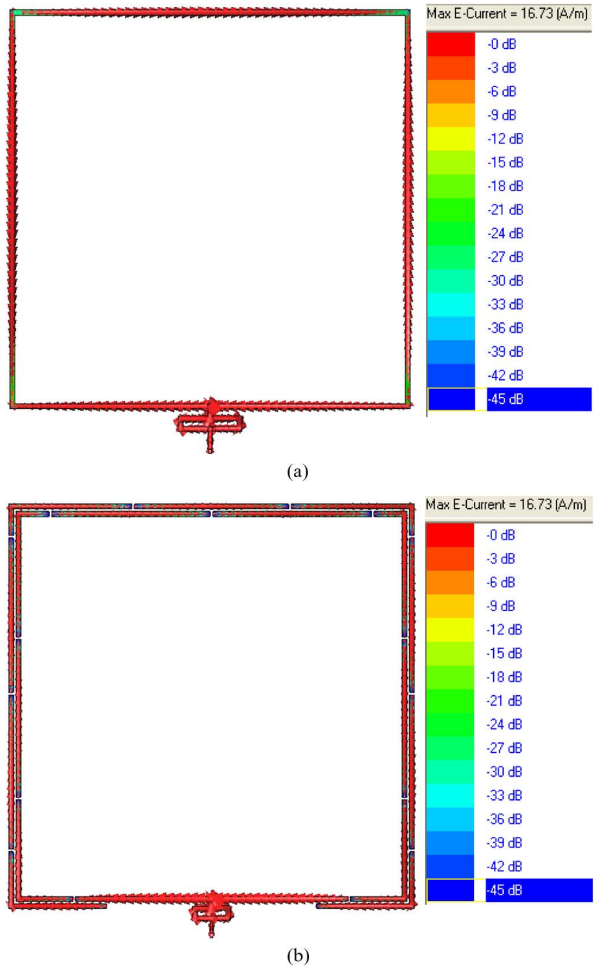

Fig. 10. Simulated current distribution at 915 MHz: (a) conventional solid-line loop antenna and (b) proposed segmented loop antenna.

size of $175 \times 180 \times 0.5\ \mathrm{mm}^3$ with a perimeter of 2.16λ and offers an interrogation zone of $154 \times 154\ \mathrm{mm}^2$ or $0.47\lambda \times 0.47\lambda$ (λ is the wavelength at 915 MHz in free space). As shown in Fig. 9(a), the antenna is fed by a parallel strip line printed on the opposite sides of the substrate. The upper/bottom parallel strips are connected to the inner/outer conductors of an SMA connector, respectively. A matching network comprising stubs is adopted to match the antenna to the 50-Ω feed line. The detailed configuration and dimensions of the antenna prototype are exhibited in Fig. 9(a). The photo of the antenna prototype is illustrated in Fig. 9(b). For comparison, a conventional solid-line loop antenna is prototyped as well. The square solid-line loop shown in Fig. 9(c) is with the identical size of the inner dash-line loop.

A. Current and Magnetic Field Distribution

Figs. 10 and 11 compare the simulated current distributions and the two-dimensional (2-D) magnetic field distributions of the conventional solid-line loop antenna and the proposed segmented loop antenna at 915 MHz, respectively. It is clear that the current on the solid-line loop antenna shows phase inversion and is out of phase in the adjacent sides of the loop. The magnetic field produced by the currents on the adjacent sides of the solid-line loop antenna cancel out each other and is thus very weak in the central portion of the interrogation zone. Instead, the segmented line configuration ensures the currents are in-phase and the magnitude of the current is almost equal along the segmented loop antenna. Such current distribution results in even magnetic field distribution over the interrogation zone of the antenna even though the perimeter of the antenna is more than two operating wavelengths.

Fig. 12 exhibits the simulated magnetic field distribution along x- and y-axes. It is observed that the magnetic field features stronger magnitude in the regions very close to the loop lines and experiences a shape reduction when the observation point moves away from the lines. Fig. 12(a) compares the magnetic field distribution of the antennas along the x-axis, which are symmetrical with respect to the y-axis for both the antennas. The segmented loop antenna offers desired magnetic field distribution with a variation of 3 dB over the major portion of the interrogation zone $(-65\ \mathrm{mm} \leq x \leq 65\ \mathrm{mm})$ while the solid-line loop antenna suffers a variation of 25 dB over the same region. Fig. 12(b) exhibits the magnetic filed distribution along the y-axis, which is slightly asymmetrical to the x-axis due to the asymmetrical antenna geometry, the attenuation, and the radiation of the coupled lines. The maximum magnetic field variation is 10.2 dB for the segmented loop antenna and 37.5 dB for the solid-line loop antenna over the range

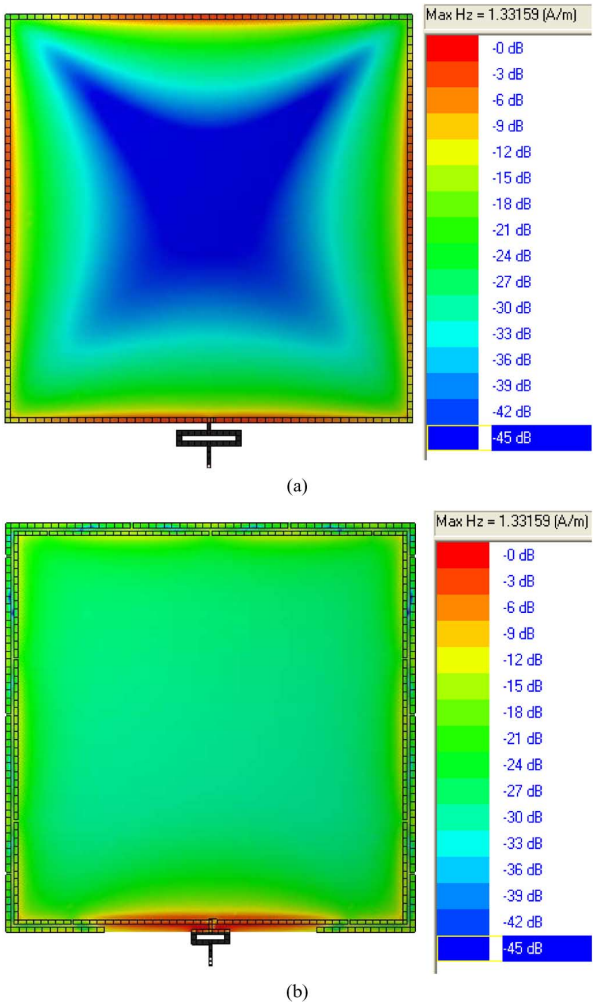

Fig. 11. Simulated 2-D magnetic field distribution at 915 MHz ($z = 0.5$ mm): (a) conventional solid-line loop antenna and (b) proposed segmented loop antenna.

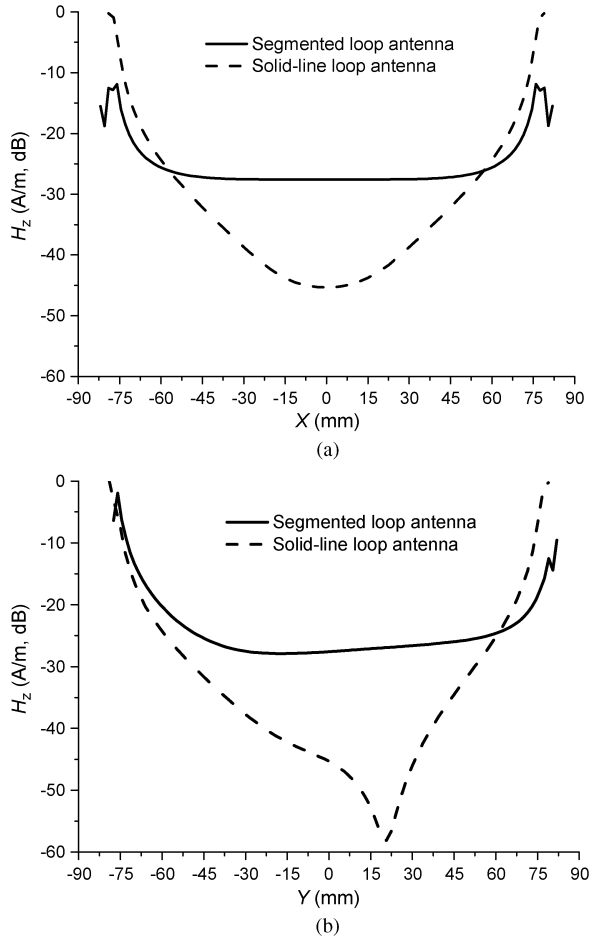

Fig. 12. Simulated magnetic field distribution of the segmented loop antenna and the conventional solid-line loop antenna (915 MHz, z = 0.5 mm): (a) x-axis variation and (b) y-axis variation.

of $-65\ \text{mm} \leq y \leq 65\ \text{mm}$. Therefore, the segmented loop antenna can generate much stronger and more even magnetic field distribution than that of the solid-line loop antenna.

Fig. 13 examines the simulated magnetic field distribution of the segmented loop antenna along x- and y- axes at 750, 840, 915, 960, and 1000 MHz, respectively. It is shown that the proposed antenna achieves the magnetic field distribution with maximum variation of 4.5 dB at the interval of $-65\ \text{mm} \leq x \leq 65\ \text{mm}$ and 12 dB over the range of $-65\ \text{mm} \leq y \leq 65\ \text{mm}$ across the frequency range of 840–960 MHz. When the frequency shifts down to 750 MHz or up to 1000 MHz, the uniformity of the magnetic field distribution degrades.

Further study shows that the current along the loop is kept in-phase at 750 MHz while the magnitude of the current suffers a large variation. The current on the sections close to the feeding port is much stronger than that on the top portion of the loop. As a result, the magnetic field in the upper zone of the antenna is weaker than that close to the feeding portion. The asymmetrical current distribution is attributed to the weak coupling between the segmented lines since they are electrically short at lower frequencies, for example 750 MHz. At higher frequencies, for instance, 1000 MHz, the current along the loop exhibits phase inversion and nulls on the loop. As a result, the magnetic field distribution shown in Fig. 13(b) shows weak field intensity in the central portion of the antenna.

Fig. 14 shows the simulated and measured magnetic field distributions of the antennas at 915 MHz. The magnetic field distributions were measured using E5230A vector network analyzer (VNA) and a near-field probe (Langer EMV-Technik RF-R 3-2) [17]. The antenna and the near-field probe are connected to the Port 1 and the Port 2 of the VNA, respectively. The relatively magnetic field intensity is quantified by $|S_{21}|$. The near-field magnetic field probe was placed on the surface of the antenna prototype, and was moved along the x- and y- axes separately with an interval of 5 mm. The calibration of the probe is not required in the measurement because the relatively field distribution instead of the absolute magnitude of the magnetic field is of interest here. Good agreement is achieved. For brevity, the results at other frequencies are not exhibited.

B. Impedance Matching

The impedance matching measurement of the antennas was carried out using the Agilent E5230A vector network analyzer. Fig. 15 shows the simulated and measured return loss. The proposed segmented loop antenna exhibits broadband impedance bandwidth, the frequency range for 10 dB return loss is from

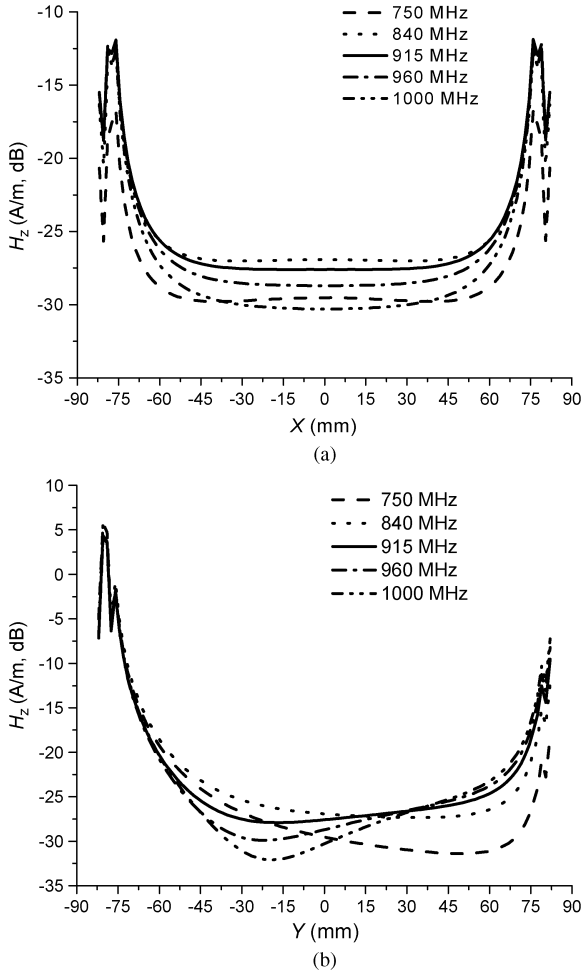

Fig. 13. Simulated magnetic field distribution of the segmented loop antenna prototype at different frequencies ($z = 0.5$ mm)s: (a) x-axis variation and (b) y-axis variation.

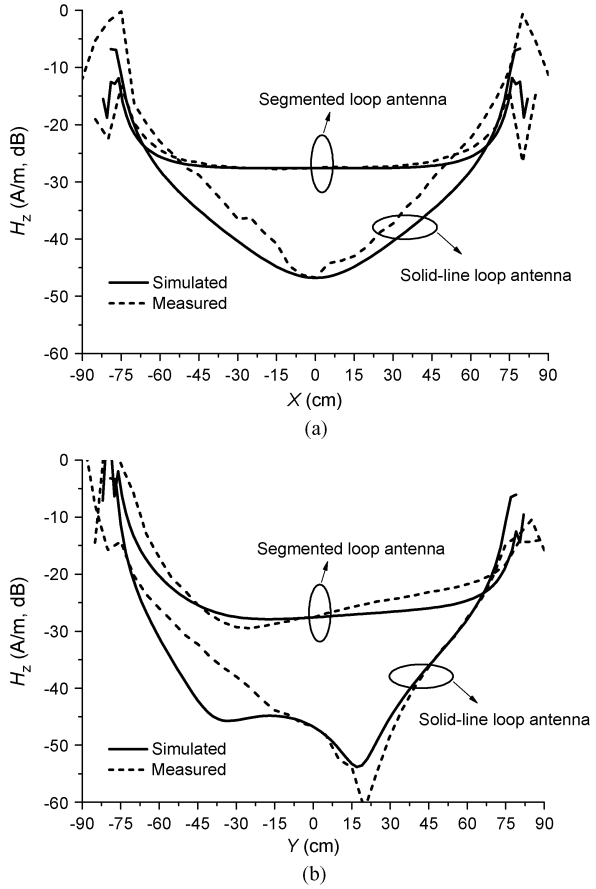

Fig. 14. Simulated and measured magnetic field distributions of the antennas (915 MHz, $z = 0.5$ mm): (a) x-axis variation and (b) y-axis variation.

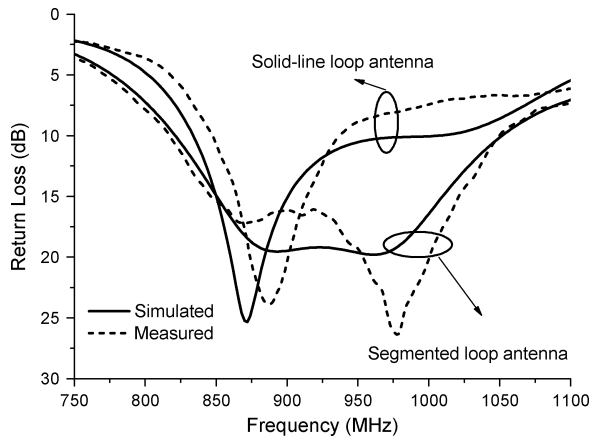

Fig. 15. Simulated and measured return loss of the antennas.

820 MHz to 1050 MHz, or 24.6%. The measured result agrees well with the simulation.

C. Reading Range

To further verify the performance of the proposed segmented loop antenna, the prototype was used as the reader antenna in a UHF near-field RFID system to detect UHF near-field tags. In a set-up shown in Fig. 16, the antenna prototype was connected to the Impinj Speedway reader operating at 865–956 MHz with 30-dBm output [18] to detect the Impinj button type tags (J21, 8 mm in diameter) [19], where 25 tags are positioned symmetrically on a Styrofoam disc with a diameter of 160 mm. The number of the correctly detected tags was recorded when the Styrofoam disc was positioned right above the antenna. To ensure the reliability of the results, the tags attached on the Styrofoam disc were randomly placed on the antenna, and an average of five tests was recoded.

The measured reading rate against the reading range is exhibited in Fig. 17. Both the proposed segmented loop antenna and the conventional solid-line loop antenna offer bi-directional detection at $\pm z$ axis of the antennas. The segmented loop antenna exhibits superior performance at each reading range. A 100% reading rate is achieved at a distance of 24 mm.

The conventional solid-line loop antenna, however, can only offer a reading rate of 45% even though the tags are placed on the surface of the antenna ($z = 0$ mm). The poor reading rate is attributed to the very weak magnetic field in the central portion of the antenna, as shown in Fig. 11(a).

D. Directional Antenna Prototype

In many RFID applications, the reader antennas with a directional detection are preferred. Fig. 18 demonstrates a directional segmented loop antenna configuration, where the

Fig. 16. Near-field RFID measurement set-up using the Impinj Speedway reader and the segmented loop antenna prototype.

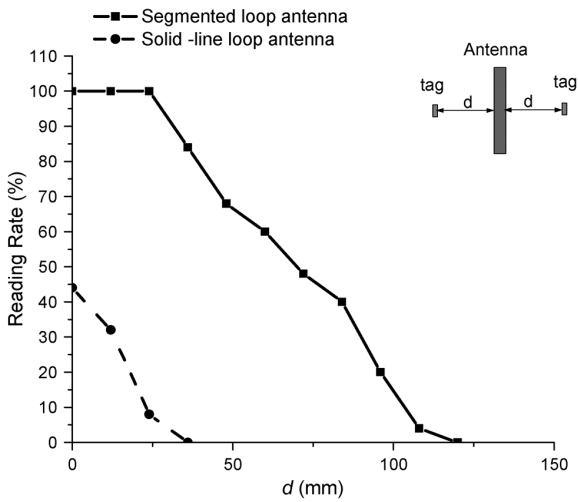

Fig. 17. Measured reading rate against reading range: segmented loop antenna and solid-line loop antenna.

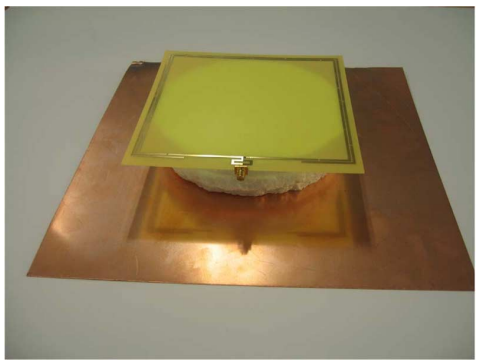

Fig. 18. Directional segmented loop antenna prototype.

proposed segmented loop antenna prototype is positioned right above a copper plate $(300 \times 300\ \mathrm{mm}^2)$ with a distance, g. The antenna is supported with a piece of Styrofoam. The measured return loss of the directional antenna prototypes is shown in Fig. 19. It is noted that the metal plate shows a severe effect on antenna impedance matching, especially when the metal plate is placed very close to the antenna.

Fig. 20 exhibits the reading rate of the directional segmented loop antenna prototype wherein the copper plate $(300 \times 300\ \mathrm{mm}^2)$ is 40 mm away from the antenna. The

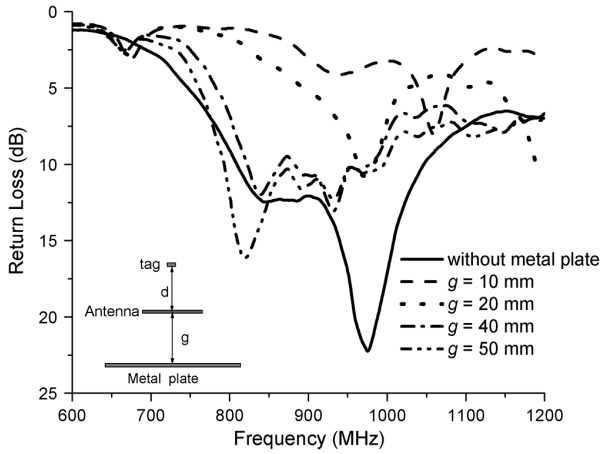

Fig. 19. Measured return loss of the directional segmented loop antenna prototypes.

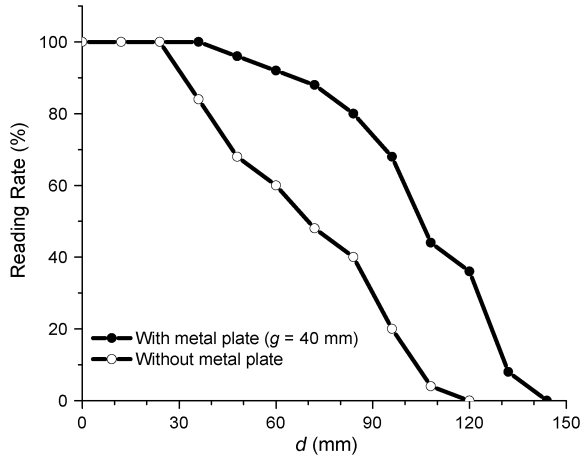

Fig. 20. Measured reading rate against reading range: directional segmented loop antenna and the original segmented loop antenna.

reading range for 100% tag detection is enhanced up to 36 mm, that is, 1.5 times that of the original segmented loop antenna prototype without the metallic reflector.

VI. Conclusions

It is a challenge to design electrically large loop-type antenna for UHF near-field RFID applications. The major design consideration is to control the phase lag of the current so that the current is kept in-phase along the loop. The proposed segmented loop antenna has demonstrated the capability of producing strong magnetic field with relatively uniform field distribution in the near-field region of the antenna even though the perimeter of the antenna is longer than two operating wavelength, which is very promising for UHF near-field RFID reader applications.

Furthermore, the investigation has shown that the proposed segmented loop antenna has produced the strongest and most even magnetic field distribution when the lengths of the segmented line sections are approximately one quarter operating wavelength. The properties of substrate supporting the antenna traces have shown significant effects on antenna performance as well.

REFERENCES

[1] R. Wantc, "An introduction to RFID technology," *IEEE Pervasive Comput.*, vol. 5, no. 1, pp. 25–33, Jan.–Mar. 2006.

[2] J. Landt, "The history of RFID," *IEEE Potentials*, vol. 24, no. 4, pp. 8–11, Oct.–Nov. 2005.

[3] K. Finkenzeller, *RFID Handbook*, 2nd ed. New York: Wiley, 2004.

[4] P. Harrop, "Near Field UHF vs. HF for Item Level Tagging" [Online]. Available: http://www.eurotag.org/?Articles_and_Publications

[5] D. Desmons, "UHF Gen2 for item-level tagging," presented at the RFID World 2006, [Online]. Available: www.impinj.com/files/Impinj_ILT_RFID_World.pdf

[6] UHF Gen 2 for Item-Level Tagging Impinj RFID technology series paper [Online]. Available: http://www.impinj.com/files/MR_GP_ED_00003_ILT.pdf

[7] C. Ajluni, "Item-level RFID takes off," *RF Design Mag.*, Sep. 2006.

[8] "Item-Level Visibility in the Pharmaceutical Supply Chain: A Comparison of HF and UHF RFID Technologies," Philips, TAGSYS, and Texas Instruments [Online]. Available: http://www.tagsysrfid.com/modules/tagsys/upload/news/TAGSYSTI-Philips White-Paper.pdf

[9] P. Cole, "Coupling Relations in RFID Systems," 2003 [Online]. Available: http://www.autoidlabs.org/publications/page.html

[10] P. V. Nikitin, K. V. S. Rao, and S. Lazar, "An overview of near field UHF RFID," in *Proc. IEEE Int. Conf. on RFID*, Mar. 2007, pp. 167–174.

[11] S. Chen and V. Thomas, "Optimization of inductive RFID technology," in *Proc. IEEE Int. Symp. on Electronics and the Environment*, May 2001, pp. 82–87.

[12] D. M. Dobkin, S. M. Weigand, and N. Iyec, "Segmented magnetic antennas for near-field UHF RFID," *Microw. J.*, vol. 50, no. 6, Jun. 2007.

[13] R. A. Oliver, "Broken-loop RFID reader antenna for near field and far field UHF RFID tags," U.S. design patent D570, 337 S, Jun. 3, 2008.

[14] R. A. Oliver, "Broken-loop RFID reader antenna for near field and far field UHF RFID tags," U.S. design patent D574, 369 S, Aug. 5, 2008.

[15] R. A. Oliver, "Broken-loop RFID reader antenna for near field and far field UHF RFID tags," U.S. design patent D574, 370 S, Aug. 5, 2008.

[16] *"IE3D User's Manual Release 12,"* Zeland Software Inc., Fremont, CA, Oct. 2006.

[17] [Online]. Available: http://www.langer-emv.de/en/products/disturbance-emission/near-field-probes/rf-1/

[18] [Online]. Available: http://www.impinj.com/products/rfid-reader.aspx

[19] [Online]. Available: http://www.rfidium.com/i/pdf/DS3_Rfidium_Inlay_J21_Button2-11-09-08.pdf

Xianming Qing (M'90) was born in China in May 1965. He received the B.Eng degree from the University of Electronic Science and Technology of China (UESTC), in 1985, and the Dr.Eng degree from Chiba University, Japan, in 2010.

During 1987–1996, he was with UESTC for teaching and research and appointed as a Lecturer in 1990 and an Associate Professor in 1995. He joined the National University of Singapore (NUS) in 1997 as a Research Scientist, where he focused on study of high-temperature superconductor (HTS) microwave devices. Since 1998, he has been with the Institute for Infocomm Research (I2R, formerly known as CWC and ICR), Singapore. He is currently holding the position of Research Scientist and the Leader of Antenna Group under the RF and Optical Department. His main research interests are antenna design and characterization for wireless applications. In particular, his current R&D focuses on small and broadband antennas/arrays for wireless systems, such as ultrawideband (UWB) systems, radio frequency identification (RFID) systems and medical imaging systems, microwave, mmW, submmW, and THz imaging systems. He has authored and coauthored over 100 technical papers published in international journals or presented at international conferences, and five book chapters. He holds eight granted and filed patents.

Dr. Qing has been a member of the IEEE Antennas and Propagation Society since 1990. He received six awards of advancement of science and technology in China. He is also the recipient of the IES Prestigious Engineering Achievement Award 2006, Singapore. He served as the Organizer and Chair for special sessions on RFID antennas at the IEEE Antenna and Propagation Symposium in 2007 and 2008. He also served as the Guest Editor of the *International Journal on Wireless & Optical Communications* Special Issue on Antennas for Emerging Radio Frequency Identification (RFID) Applications. He has served as the TPC member and Session Chair for a number of conferences, and as a Reviewer for many prestigious journals such as IEEE T-AP, T-MTT, IEEE-AWPL, MWCL, IET-MAP, *Electronics Letters*, etc.

Chean Khan Goh received the B.Eng. degree from Multimedia University, Malaysia, in 2007 and the M.Eng. degree from National University of Singapore, in 2009.

He worked as a Research Officer in the Institute for Infocomm Research, Singapore, from 2007 to 2010. His research interests include antennas for RFID application and antenna impedance measurement methodology.

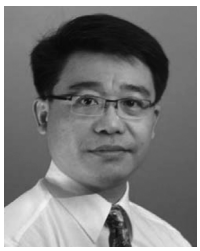

Zhi Ning Chen (F'08) received the B.Eng., M.Eng., and Ph.D. degrees from the Institute of Communications Engineering, China, in 1985, 1988, and 1993, respectively, and the DoE degree from the University of Tsukuba, Japan, in 2003, all in electrical engineering.

During 1988 to 1997, he worked at the Institute of Communications Engineering, Southeast University, and City University of Hong Kong, China, with teaching and research appointments. In 1997, he was awarded a JSPS Fellowship to join the University of Tsukuba, Japan. In 2001 and 2004, he visited the University of Tsukuba under a JSPS Fellowship Program (senior level). In 2004, he worked at the IBM T. J. Watson Research Center, New York, as an Academic Visitor. Since 1999, he has worked at the Institute for Infocomm Research, Singapore, where his current appointments are Principal Scientist and Department Head for RF & Optical. He is concurrently holding Adjunct/Guest Professors at Southeast University, Nanjing University, Shanghai Jiao Tong University, Tongji University and the National University of Singapore. He has published 280 journal and conference papers as well as authored and edited the books entitled *Broadband Planar Antennas, UWB Wireless Communication, Antennas for Portable Devices*, and *Antennas for Base Station in Wireless Communications*. He also contributed to the books *UWB Antennas and Propagation for Communications, Radar, and Imaging* as well as *Antenna Engineering Handbook*. He holds 28 granted and filed patents with 17 licensed deals with industry. His current research interest includes applied electromagnetics, antennas for applications of microwave, mmW, submmW, and THz in imaging systems.

Prof. Chen is a Fellow of the IEEE for his contribution to small and broadband antennas for wireless and an IEEE AP-S Distinguished Lecturer (2008–2010). He is the recipient of the CST University Publication Award 2008, IEEE AP-S Honorable Mention Student Paper Contest 2008, IES Prestigious Engineering Achievement Award 2006, I2R Quarterly Best Paper Award 2004, and IEEE iWAT 2005 Best Poster Award. He has organized many international technical events as key organizer. He is the founder of International Workshop on Antenna Technology (iWAT).